Received: 19 October 2022 | Revised: 21 December 2022 | Accepted: 22 December 2022

DOI: 10.1111/ijac.14332

International Journal of Applied Ceramic Technology

RESEARCH ARTICLE

Application of factorial model for an optimization of partial replacement of feldspar by talc on the sintering process

Robson Couto da Silva[1] | **Felipe de Almeida La Porta**[2] | **Graciela Aparecida dos Santos Silva**[3] | **Renato Mandalozzo Tebcherani**[4] | **Evaldo Toniolo Kubaski**[1] | **Estevam Augusto Bonfante**[5] | **Sergio Mazurek Tebcherani**[3,6]

[1]Department of Materials Engineering, State University of Ponta Grossa (UEPG), Ponta Grossa, Paraná, Brazil

[2]Laboratory of Nanotechnology and Computational Chemistry, Federal University of Technology – Paraná, Londrina, Paraná, Brazil

[3]Department of Chemistry, State University of Ponta Grossa (UEPG), Ponta Grossa, Paraná, Brazil

[4]Department of Medicine, State University of Ponta Grossa (UEPG), Ponta Grossa, Paraná, Brazil

[5]Department of Prosthodontics and Periodontology, Bauru School of Dentistry, University of São Paulo, Bauru, São Paulo, Brazil

[6]Department of Production Engineering, Federal University of Technology – Paraná, Ponta Grossa, Paraná, Brazil

Correspondence
Robson Couto da Silva, Department of Materials Engineering, State University of Ponta Grossa (UEPG), Ponta Grossa, PR, Brazil.
Email: rcsilva@uepg.br; robson.materiais@gmail.com

Funding information
Conselho Nacional de Desenvolvimento Científico e Tecnológico, Grant/Award Numbers: 304675/2016-4, 313484/2019-8

Abstract

This research used a factorial model containing two levels and three variables to evaluate the partial substitution of sodium feldspar (albite) by a talc ore found in abundance in the region of Itaiacoca—Brazil. The model can also be used to verify the influence of initial talc particle size, proportion, and sintering threshold temperature on the following physical properties, such as linear shrinkage, water absorption, bulk density, total porosity, and firing color. In this study, the mechanical strength of the compositions was evaluated by the flexural strength test. The factorial model indicated the sintering temperature as the variable that most affects the samples' densification and the proportion of talc as the variable that changes the firing color. The experiment that used a higher sintering temperature combined with a coarser talc granulometry presented the highest mechanical strength. When more refined granulometry was used, there was the beginning of an overfire process. Water absorption values in the range of .04% and modulus of rupture of 49 MPa were obtained, confirming the talc's effectiveness as a secondary flux agent suitable for the formulation of ceramic bodies.

KEYWORDS
factorial design, granulometry, sintering temperature, talc

1 | INTRODUCTION

The worldwide consumption of raw materials for the manufacture of ceramic artifacts has been growing annually,[1] with alkaline feldspar being the conventionally used fluxes.[2,3] The flux agents function is the production of the liquid phase during sintering,[4] which provides the densification and closing of pores and consequently greater mechanical strength to the finished product.

Gulgonul et al. reported that high-quality sodium and potassium feldspar deposits are running out.[5] In 2018, for example, it was estimated that the consumption of feldspar materials was close to 29 million tons. Therefore, to maintain a secure supply of this resource, the use of alternative raw materials should be increased.[6] A notable example of this is, of course, the use of mixed deposits such as granites or granite pegmatites to maintain a high-quality supply of potassium feldspar.[7]

Talc is a metamorphic phyllosilicate[8] referenced as a hydrated magnesium silicate composed of a magnesium-hydroxyl octahedral (brucite) sheet sandwiched among two sheets of tetrahedral silicon–oxygen with the chemical formula $Mg_3Si_4O_{10}(OH)_2$.[9,10] Brazil, China, and the United States are the world's largest producers, and it is estimated that about 22% of the talc sold in the United States is used in ceramics.[11]

Torres et al.[12] proved the effectiveness of talc in increasing the liquid phase from its partial fusion. New phases were observed with the elevation of temperature as the SiO_4 tetrahedrons rearranged. Particularly, the dehydroxylation process of talc started at about 850°C, leading to the appearance of an amorphous phase, whereas, at 1000°C, occurs the formation of the protoenstatite structure.[12] However, oxygen from this reaction can create new arrangements with the amorphous phase and initiate the nucleation of enstatite, which predominates at 1200°C.[12]

Several kinds of research present more significant densification and improvement in the mechanical properties of ceramic materials due to the addition of talc at temperatures in the range of 1200°C. For example, Sánchez et al. also observed reduced water absorption and a reduction in pyroplastic deformation of the compositions studied.[13]

Mukhopadhyay et al. pointed out that the best results are obtained in talc additions in the range of 3% by weight.[14] Serra et al.[15] studied typical triaxial compositions of porcelain and verified greater densification in compositions containing talc in conjunction with potassium feldspar concerning additions of other secondary flux agents such as spodumene and calcite. In addition, a reduction of about 15% in porosity at 1200°C was observed when comparing a composition containing talc with another that used only feldspar as the flux agent.[15]

This work sought to evaluate the effectiveness of talc from the district of Itaiacoca—Brazil, as a partial substitute for sodium feldspar from a factor model, as well as to verify the influence of the granulometry and the sintering threshold temperature on the functional properties of a ceramic paste containing raw materials for the production of porcelain.

2 | MATERIALS AND METHODS

In this study, statistical factorial design (.05 significance) was used to evaluate the compositions' responses containing raw materials: Itajara talc, from the region of Itaiacoca—Brazil, Marc albite, and Oxford kaolin. These raw materials were analyzed via X-ray fluorescence in a Shimadzu model EDX 700 equipment with a detection limit of .001%. To carry out the test on the raw materials, samples already processed in 200 mesh Tyler were used.

The kaolin and albite were dried and processed in 200 mesh Tyler, and the talc was processed in 20 and 200 mesh Tyler. The compositions after grinding were analyzed in wet analysis in Cilas 920 laser granulometer with a detection limit of .3 μm. For this test, 200 mg of each were de-agglomerated in ultrasound for 60 s and then tested in the equipment.

For the compositions' preparation, wet milling was performed in an eccentric mill Servitech model CT-12242 for 10 min at a rotation of 400 rpm. In the grinding process, a porcelain jar with an alumina coating with a capacity of 300 ml was used. The grinding elements were alumina spheres with diameters of 12 and 20 mm in proportions of approximately 80% and 20%, respectively, which occupied approximately 50% of the useful volume of the jar. An amount of 100 g of the composition was placed in the jar, and then water was added until there was a free volume in the jar of approximately 25%. After grinding, it was dried in an oven until constant mass. Finally, the material was sieved in 80 mesh Tyler and pressed with about 6% moisture in a 50 mm diameter mold at a compression pressure of 4.5 MPa.

For the sintering process, a Jung model LF 7012 electric muffle furnace was used. The firing cycles used were established with sintering temperature thresholds of 1170 and 1220°C, always using the constant heating rate at 10°C/min, from room temperature, with a sintering threshold of 10 min, the cooling occurred under normal oven conditions.

A factorial design was studied, containing 2^3 (two levels and three variables). The design was executed in duplicate. The responses analyzed in the experiments were linear shrinkage (L_s), water absorption (W_a), bulk density (D_{bulk}), total porosity (P_{total}), determined by Equations (1)–(4), and color difference (dE) from Cielab coordinates (using calcined alumina and samples obtained in experiment 1 as standard). To determine the Cielab coordinates, a colorimeter of Delta Colorium was used utilizing the Lab 7 Gold software, with the measurements in triplicate.

TABLE 1 Nomenclature, levels, and codes of the variables used in the statistical model

	Talc proportion (%)		Talc initial particle size (mesh Tyler)		Temperature (°C)	
Nomenclature	Talc		Size		Temp	
Level	10	20	20	200	1170	1220
Code	−	+	−	+	−	+

The true density determination (D_{true}) of the material was obtained in a Quantachrome Instruments helium pycnometer, model Ultrapycnometer 1000:

$$L_s = \frac{(L_g - L_f)}{L_g} \cdot 100 \quad (1)$$

$$W_a = \frac{(M_w - M_d)}{M_d} \cdot 100 \quad (2)$$

$$D_{bulk} = \frac{M_d}{M_w - M_i} \quad (3)$$

$$P_{total} = \left(1 - \frac{D_{geom}}{D_{true}}\right) \cdot 100 \quad (4)$$

$$D_{geom} = \frac{M_d}{V_d} \quad (5)$$

where L_g (cm) is the length of the green specimen after drying; L_f (cm) is the length of the fired specimen; M_w (g) is the mass of the wet specimen after firing (immersion for 24 h in water); M_i (g) is the mass of the immersed specimen after firing (Archimedes method); M_d (g) is the mass of the dry specimen after firing; D_{geom} (g/cm^3) is the geometrical density of the specimen; V_d (cm^3) is the geometric volume of the dry body after firing (length × width × height); D_{true} (g/cm^3) is the true density from helium pycnometry.

The percentages of talc in partial replacement of albite, the initial talc particle size, and the sintering threshold temperature were established as factorial design variables. For this, a constant proportion of kaolin of 30% over dry mass was established. The percentage of talc varying between 10 and 20 of the total mass in substitution for albite, with mass compositions remaining:

1. Kaolin = 30%
   Albite = 60%
   Talc = 10%

1. Kaolin = 30%
   Albite = 50%
   Talc = 20%

The levels of the variables, their respective codes, and nomenclatures in the statistical experiment are shown in Table 1.

In addition to the answers analyzed in the experiment, other parameters of the obtained compositions were also measured: loss on ignition (LOI), skeletal density (D_{skel}), geometric density (D_{geom}), open porosity (P_{open}), and closed porosity (P_{closed}). The formulas used for the calculations are presented in the following equations:

$$LOI = \frac{(M_g - M_d)}{M_g} \cdot 100 \quad (6)$$

$$D_{skel} = \frac{M_d}{M_d - M_i} \quad (7)$$

$$P_{open} = \frac{M_w - M_d}{M_w - M_i} \cdot 100 \quad (8)$$

$$P_{closed} = P_{tot} - P_{open} \quad (9)$$

where M_g (g) is the mass of the green specimen after drying.

The compositions were also tested for their mechanical strength to bending in a SHIMADZU model AUTOGRAPH AGS equipment. For this purpose, specimens were made in a rectangular mold measuring 50 × 25 mm^2. The samples were processed under the same conditions foreseen by the factorial model. The test speed used was .5 mm/min according to ASTM C1161-18. For the calculation of the modulus of rupture (MOR) of a sample with a rectangular cross-section, Equation (10) was used. Finally, these results were compared from statistical Tukey's model analysis using a Minitab software version 17.

$$\sigma = \frac{3.F.L}{2.w.h^2} \quad (10)$$

where σ (MPa) is the MOR; F (N) is the breaking force; L (m) is the length between supports; w (m) is the width of the sample; h (m) is the height of the sample.

The phases formed during the sintering process were determined by X-ray diffraction (XRD) in a Rigaku Ultima IV XRD with Cu K_α radiation equipment. It was used at a 1°/min scan speed operating at 40 kV and 30 mA and 2θ ranging from 10° to 110°, at a .02° step, with a divergent slit of .5°, spreading slit of .5°, and receiving slit of .3°. The results were analyzed using the Crystallographica Search-Match software version 2.1.1.1 with PDF2 database.

The microstructure of the sintered specimens and their respective chemical analyzes was evaluated by

TABLE 2 Chemical analysis of raw materials used (%wt.)

	Na_2O (%)	K_2O (%)	MgO (%)	CaO (%)	Al_2O_3 (%)	Fe_2O_3 (%)	SiO_2 (%)	TiO_2 (%)
Kaolin	–	1.988	–	–	37.784	1.043	58.838	.347
Albite	6.889	1.274	–	1.810	18.437	.137	71.453	–
Talc	–	.336	25.725	1.334	4.905	2.167	65.255	.277

TABLE 3 Results of granulometric analysis of factor model compositions

Experiment	Talc (%)	Size (mesh)	*T* (°C)	*D*10 (μm)	*D*50 (μm)	*D*90 (μm)	Average diameter (μm)	Arrangement
1	−	−	−	1.48	11.97	49.15	19.58	Bimodal
2	+	−	−	1.52	12.10	50.70	20.15	Bimodal
3	−	+	−	1.48	12.14	49.27	19.70	Bimodal
4	+	+	−	1.50	11.80	49.10	19.53	Bimodal
5	−	−	+	1.48	11.97	49.15	19.58	Bimodal
6	+	−	+	1.52	12.10	50.70	20.15	Bimodal
7	−	+	+	1.48	12.14	49.27	19.70	Bimodal
8	+	+	+	1.50	11.80	49.10	19.53	Bimodal

field emission gun scanning electron microscopy and chemical microanalysis by energy-dispersive X-ray spectroscopy (EDS) in Mira 3/Tescan model equipment. For the microstructural analysis, the sintered samples were attacked with a 5% solution of hydrofluoric acid for 60 s to remove the vitreous phase. These samples were washed in running water after the attack and oven-dried at 105°C. For the chemical analysis, samples without any kind of attack to preserve their chemical composition after sintering were used. Later, their surfaces were covered with a layer of gold.

3 | RESULTS AND DISCUSSION

3.1 | X-ray fluorescence and particle size analysis

Table 2 presents the results obtained in X-ray fluorescence analysis.

Table 2 shows that the talc used has an MgO content within the talc range used in other research.[16,17] However, the other raw materials' chemical composition also matches the oxide contents usually found in other studies.[18]

Table 3 presents the results of granulometric analysis of the compositions used in this work. The starting granulometry of the talc and the proportion used in the composition did not bring any change in the granulometric arrangement in the detection range of the equipment. Moreover, refined granulometry was obtained in all compositions, which is fundamental so that the particles could react more quickly, that is, leading to a significant improvement in the speed of sintering.[19]

3.2 | Physical characterization and factorial model

Table 4 indicates the average results obtained from the characterization tests for the experiments proposed by the statistical model.

Table 5 shows the calculated effects and their respective interactions and significance for the statistical experiment, with the highlighted values referring to statistically significant responses.

Figure 1 shows the results of the calculated effects and their respective interactions and significance for linear shrinkage. The temperature caused a significant impact on the linear shrinkage, whereas the other variables and interactions did not produce statistically significant changes. The results in Table 5 indicate that the increase in temperature from 1170 to 1220°C caused an increase in the firing retraction, increasing it by 1.88%. These results occur because higher temperature provides more thermal energy to the system, allowing: a more significant liquid phase formation, therefore causing densification, closure of pores, and consequently retraction of the material.[20] Another factor contributing to this is that magnesium oxide contributes to forming the liquid phase from 1180°C, as verified in other works.[13,16]

This result is corroborated by the water absorption and bulk density data presented in Table 5 and Figure 2A,B.

TABLE 4 Average responses obtained in the statistical model for each tested experiment

Experiment	Talc (%)	Size (mesh)	Temp (°C)	L_s [a] (%)	W_a [a] (%)	D_{bulk} [a] (g/cm^3)	P_{total} [a] (%)	$dE_{alumina}$ [a,b]	$dE_{experiment1}$ [a,c]
1	−	−	−	12.39 ± .72	3.23 ± .62	2.22 ± .04	12.40 ± 1.40	34.47 ± .65	.00 ± .00
2	+	−	−	12.25 ± .78	2.76 ± 1.55	2.25 ± .07	11.08 ± 2.90	37.75 ± 1.10	3.28 ± 1.10
3	−	+	−	11.30 ± .99	3.18 ± 1.06	2.22 ± .05	12.25 ± 2.02	36.08 ± 1.88	1.61 ± 1.88
4	+	+	−	13.05 ± .28	6.03 ± 1.88	2.09 ± .07	18.62 ± 2.67	36.48 ± .74	2.01 ± .74
5	−	−	+	14.40 ± 1.34	.04 ± .02	2.35 ± .00	2.44 ± .04	35.43 ± 1.53	.96 ± 1.53
6	+	−	+	13.55 ± 1.70	.13 ± .01	2.35 ± .00	1.47 ± .09	36.76 ± 1.34	2.29 ± 1.34
7	−	+	+	14.40 ± .49	.08 ± .01	2.35 ± .01	2.77 ± .32	35.86 ± .18	1.39 ± .18
8	+	+	+	14.15 ± 1.91	.07 ± .02	2.36 ± .01	2.23 ± .22	37.10 ± .32	2.63 ± .32

[a]Average response obtained from the experiment in duplicate.
[b]$dE_{alumina}$ refers to alumina used as standard.
[c]$dE_{experiment1}$ refers to samples from experiment 1 used as standard.

TABLE 5 Calculated effects and interactions for linear shrinkage (L_s), water absorption (W_a), bulk density (D_{bulk}), total porosity (P_{total}), and color difference (dE) for statistical experiment

Effect	L_s (%)	W_a (%)	D_{bulk} (g/cm^3)	P_{total} (%)	dE
Average	13.19 ± .29	1.94 ± .24	2.27 ± .01	7.91 ± .41	36.24 ± .28
Talc	.13 ± .58	.62 ± .48	−.02 ± .02	.88 ± .82	**1.56 ± .56**
Size	.08 ± .58	.80 ± .48	−.03 ± .02	**2.12 ± .82**	.28 ± .56
Temp	**1.88 ± .58**	**−3.72 ± .48**	**.16 ± .02**	**−11.36 ± .82**	.09 ± .56
Talc × size	.62 ± .58	.81 ± .48	−.04 ± .02	**2.03 ± .82**	−.74 ± .56
Talc × temp	−.68 ± .58	−.58 ± .48	.03 ± .02	−1.64 ± .82	−.28 ± .56
Size × temp	.22 ± .58	−.81 ± .48	.04 ± .02	−1.57 ± .82	.11 ± .56
Talc × size × temp	−.32 ± .58	−.86 ± .48	.04 ± .02	−1.82 ± .82	.70 ± .56

Note: The results in bold indicate the significant variables and interactions.

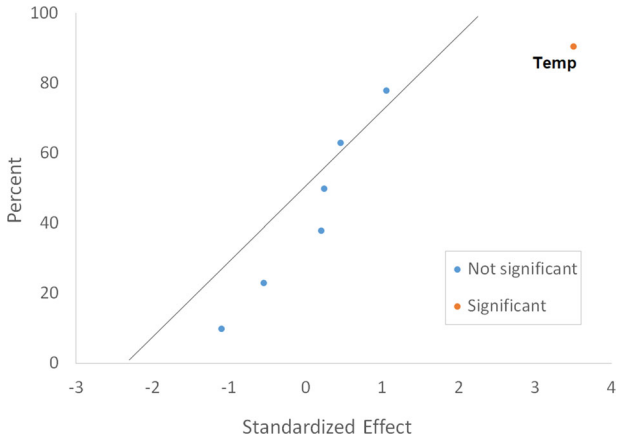

FIGURE 1 Normal effect plot (.05 significance) for statistical experiment. Effects for the linear shrinkage

From these results, the temperature increase reduced the water absorption by 3.72% and densified the compositions by about .16 g/cm^3. It is also noticeable that as well as what occurred for burn retraction, the other variables and interactions also did not cause any significant effect in the samples. The total porosity variable influenced the initial: talc granulometry, temperature, and an interaction between the talc proportion and its initial granulometry as significant effects, as shown in Figure 3.

The effect of the variable temperature promoted a reduction of about 11.36% in porosity (Table 5); this is related to densification due to a more liquid phase formed, as explained above. However, in the case of initial granulometry and talc proportion, as there is an interaction between these two variables, the interpretation of the effect caused should not be carried out individually but considering the interaction between the variables,[21] which is represented in Figure 4.

In part I of Figure 4, the increase of the initial mesh of the sieve from 20 to 200 mesh does not cause changes in the total porosity when working with 10% talc. However, when the proportion of talc is increased to 20%, the more refined grain size causes a sharp increase in the material's total porosity.

Part II of Figure 4 indicates that when the talc proportion is increased from 10% to 20%, there is a less pronounced reduction in the total porosity when working with a coarser initial grain size. However, this increase in the proportion of talc, when applied in a more refined

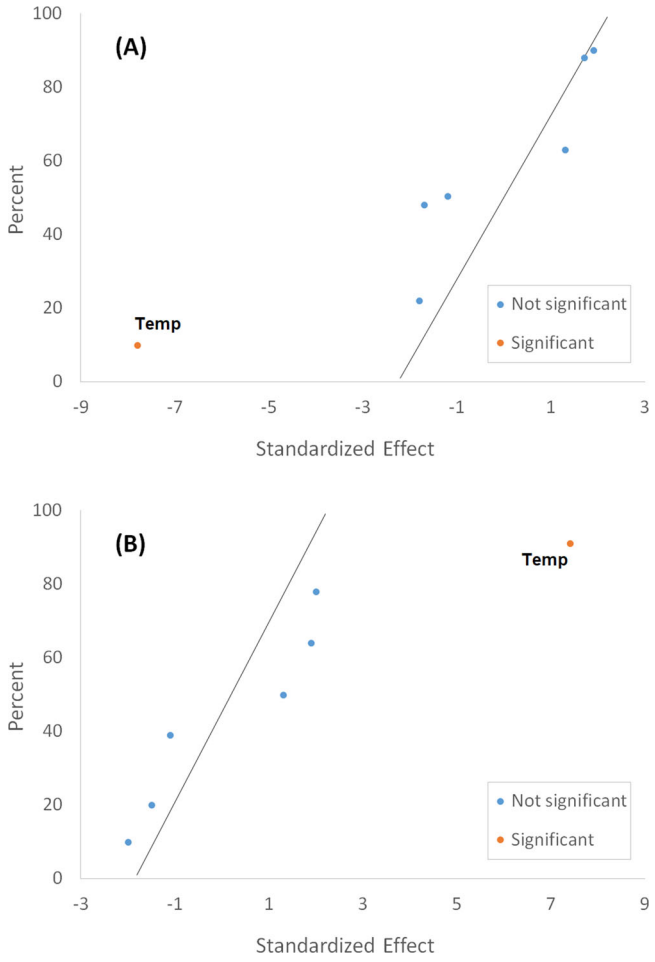

FIGURE 2 Normal effect (significance .05) for statistical experiment. (A) Effects for water absorption (B) effects for bulk density

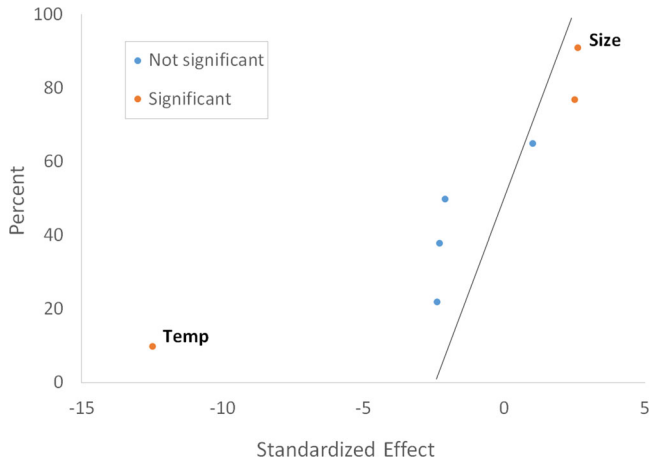

FIGURE 3 Normal effect plot (.05 significance) for statistical experiment. Effect for total porosity

initial grain size, presents an inverse effect; it increases the total porosity in a more accentuated way.

The explanation for this behavior is probably related to the fact that the more refined initial particle size has produced different packings of the particles in the compositions. This situation occurred in a particle size range below the detection limit of the laser particle size analyzer. Thus, the compositions with initial granulometry of the most refined talcum in the experiment of firing at 1220°C decreased the temperature of liquid phase formation and with this occurred the principle of the phenomenon of overfire, responsible for the elevation in porosity.

Bernasconi et al. found that the size of quartz grains was the parameter that most influenced the expansion of the glass phase matrix.[22] Our results indicate a similar behavior concerning talc granulometry.

Güngör et al. used a factorial model to study the factors that most affect the production of porcelain and highlight the importance of submicronic particles in the sintering speed, in which there is greater densification by reducing the diffusion distances among the particles.[19] The other physical characterization parameters performed in the samples were also analyzed and are presented in Table 6.

These results show that lesser densified samples are obtained when sintered at about 1170°C and with porosity reduction when a plateau of 1220°C is used. However, the few variations in the density and porosity values indicate that the other parameters have little influence on their properties, except for experiment 4, where a higher proportion of more refined talc allied to a lower firing temperature ended up providing the worst gresification among all the samples.

Figure 5 shows the calculated effects and their respective interactions and significance for the color difference, together with the values in Table 5. The increase in the proportion of talc is the only variable that causes a significant effect on the color difference, confirmed by the chemical composition shown in Table 2, where talc is the material with the highest iron oxide content among the raw materials used. The titanium and calcium oxides present in talc also contribute to the alteration of the samples' color. They act together with iron oxide and can make the color more yellowish or pink, respectively.[1]

Figure 6 shows the samples obtained for the eight experiments studied in the factorial model.

Figure 7 shows the normal graphics of the residues to check the factorial model's validity. When residue values are close to the line, one can affirm that the model used is valid.[21] According to Figure 7, the experiment's values were close to the line, that is, indicating the validity of the experiment performed.

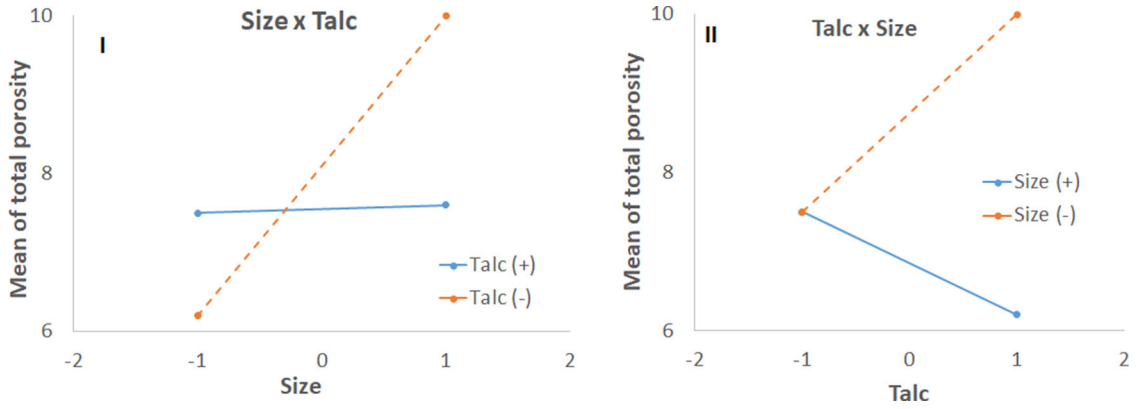

FIGURE 4 Interaction between initial talc granulometry variables and talc proportion in relation to total porosity

TABLE 6 Result of the physical characterization of the tested samples

Experiment	Talc (%)	Size (mesh)	Temp (°C)	LOI[a] (%)	D_{skel}[a] (g/cm^3)	D_{geom}[a] (g/cm^3)	P_{open}[a] (%)	P_{closed}[a] (%)
1	−	−	−	3.71 ± .08	2.39 ± .01	2.14 ± .03	7.14 ± 1.26	5.26 ± .14
2	+	−	−	4.20 ± .06	2.39 ± .01	2.14 ± .04	6.14 ± 3.28	4.93 ± .38
3	−	+	−	3.90 ± .14	2.39 ± .00	2.13 ± .06	7.04 ± 2.19	5.21 ± .18
4	+	+	−	4.30 ± .03	2.39 ± .02	2.02 ± .06	12.55 ± 3.52	6.07 ± .85
5	−	−	+	3.87 ± .13	2.35 ± .00	2.22 ± .03	.10 ± .06	2.34 ± .09
6	+	−	+	4.23 ± .03	2.36 ± .00	2.24 ± .01	.31 ± .03	1.16 ± .12
7	−	+	+	3.79 ± .00	2.36 ± .01	2.25 ± .01	.19 ± .02	2.58 ± .34
8	+	+	+	3.70 ± .80	2.36 ± .01	2.28 ± .05	.17 ± .05	2.07 ± .17

Abbreviation: LOI, loss on ignition.
[a]Average response obtained from the experiment in duplicate.

3.3 | Mechanical strength

Table 7 demonstrates the modulus values of mechanical strength to bending obtained for the samples of the factorial model experiments.

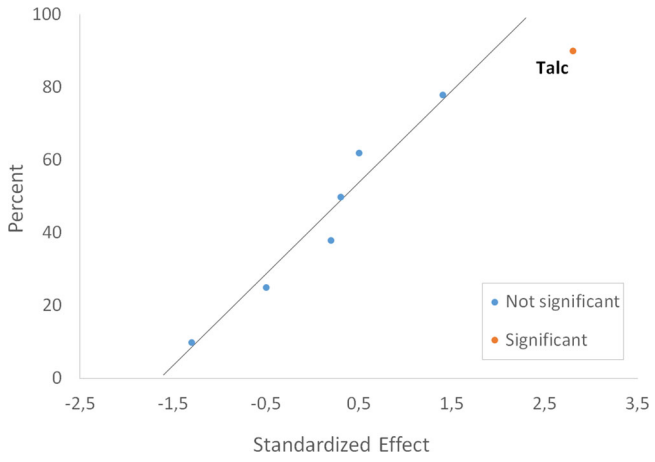

FIGURE 5 Normal effect plot (.05 significance) for statistical experiment. Effects for color difference

TABLE 7 Results of flexural strength test

Experiment	Talc (%)	Size (mesh)	Temp (°C)	MOR* (MPa)
1	−	−	−	19.21 ± 2.72[a]
2	+	−	−	13.57 ± 1.57[a]
3	−	+	−	38.52 ± 3.79[b]
4	+	+	−	28.11 ± 2.65[c]
5	−	−	+	49.04 ± 3.25[d]
6	+	−	+	38.78 ± 4.51[b]
7	−	+	+	33.82 ± 1.17[b,c]
8	+	+	+	4.44 ± .59[b]

Abbreviation: MOR, modulus of rupture.
*Average response obtained for $n = 3$. Values with equal letter do not differ for a 95% confidence level (Tukey test).

It is noticeable that the lowest mechanical strength among the samples was obtained for the sintering temperature of 1170°C allied to the initial passing granulometry of talc of 20 mesh Tyler (experiments 1 and 2). The talc's most refined initial granulometry has promoted mechanical strength to 1170°C (experiments 3 and 4). However, in 1220°C, the composition that presented the greatest

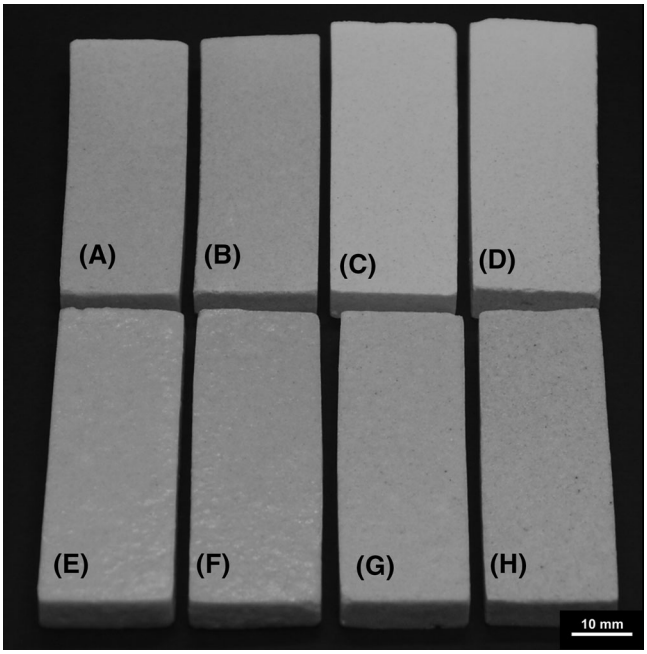

FIGURE 6 Samples studied in factorial model: (A) experiment 3; (B) experiment 4; (C) experiment 1; (D) experiment 2; (E) experiment 7; (F) experiment 8; (G) experiment 5, and (H) experiment 6

MOR was experiment 5 in which the initial granulometry was coarser. This probably occurred because in the higher temperature allied to the more refined initial grain size (experiments 7 and 8), there was the principle of overfire process, as verified in the statistical model, which contributed to a drop in the strength of the material.

It is interesting to note that although open porosity is the most harmful characteristic of mechanical strength,[23] for a temperature of 1170°C where there is still less glass phase formation, the arrangement promoted by the most refined initial granulometry minimized this effect. Thus, experiments 3 and 4, although more porous, showed MOR in the ranges in experiments 6–8.

It is also possible to verify by comparing experiments 3 with 4 and 5 with 6 that the talc proportion's elevation from 10% to 20% was detrimental to mechanical strength. Although talc tends to reduce melting temperature and increase strength, as reported in some surveys,[11,13,14] its excess may reduce mechanical strength by reducing the amount of mullite formed. Furthermore, this type of response has also been proven in other research, where it was found that talc decreased MOR.[16]

3.4 | X-ray diffraction

The XRD analysis diffractograms for all experiments are shown in Figures 8 and 9.

Only the quartz and albite phases were found in all analyzed samples (PDF card numbers 89-8939 and 1-739, respectively). It is possible to verify that in experiments 1, 2, 3, and 4, in which a lower sintering temperature was used, there is a higher proportion of crystalline phases, which is demonstrated by the higher intensity peaks of the diffractograms (Figure 8).

In samples sintered at a higher temperature, there is a lower crystallinity of the phases, which is reflected in the

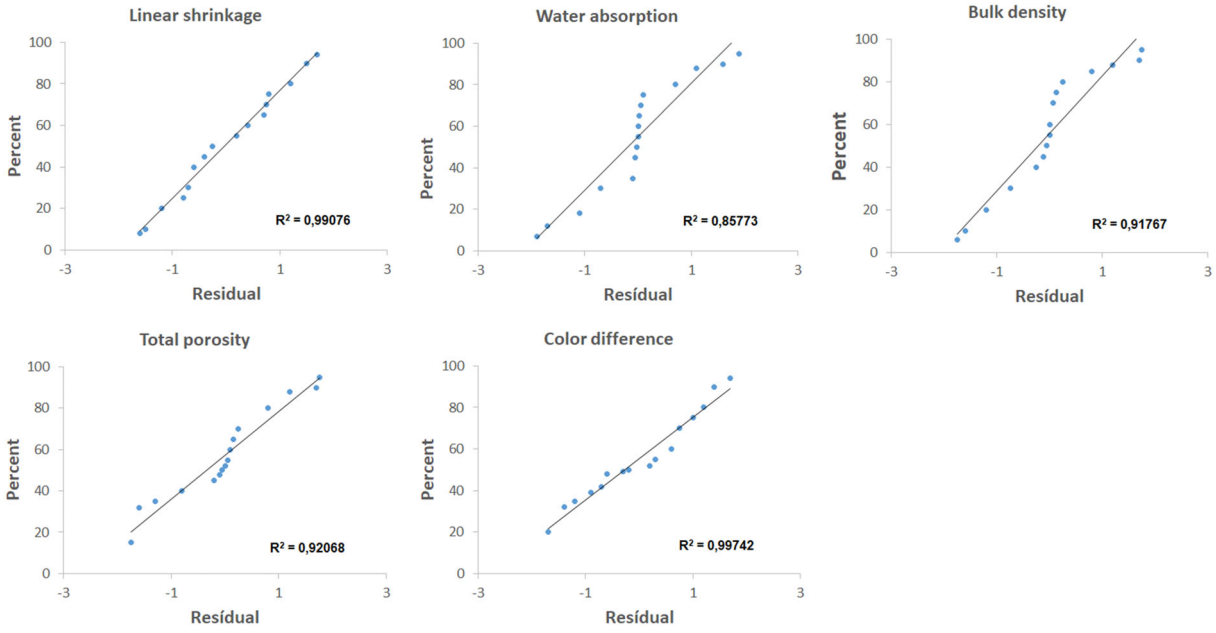

FIGURE 7 Normal residual value chart for the factorial model proposed in this survey

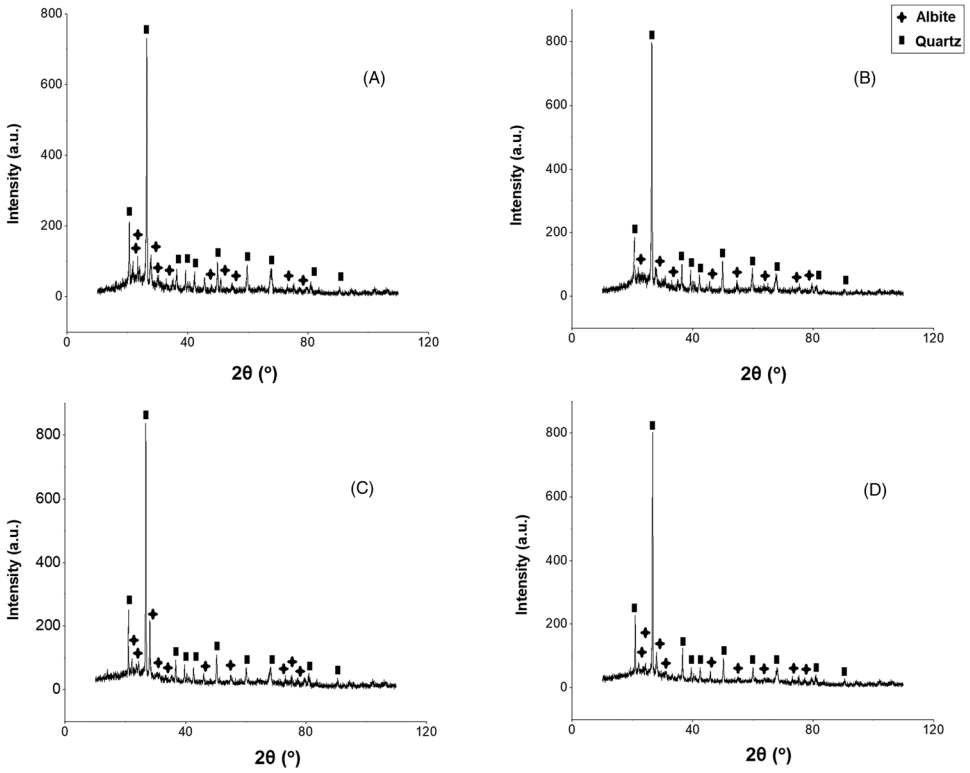

FIGURE 8 X-ray diffraction (XRD) of the porcelains obtained in this study: (A) experiment 1; (B) experiment 2; (C) experiment 3; and (D) experiment 4

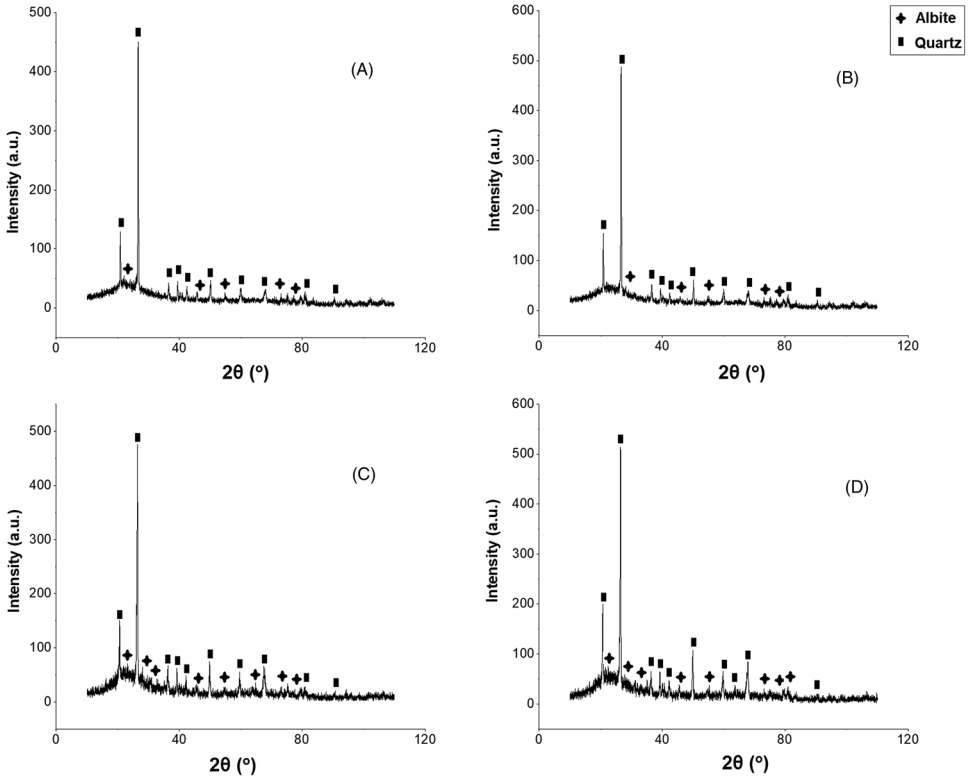

FIGURE 9 X-ray diffraction (XRD) of the porcelains obtained in this study: (A) experiment 5; (B) experiment 6; (C) experiment 7; and (D) experiment 8

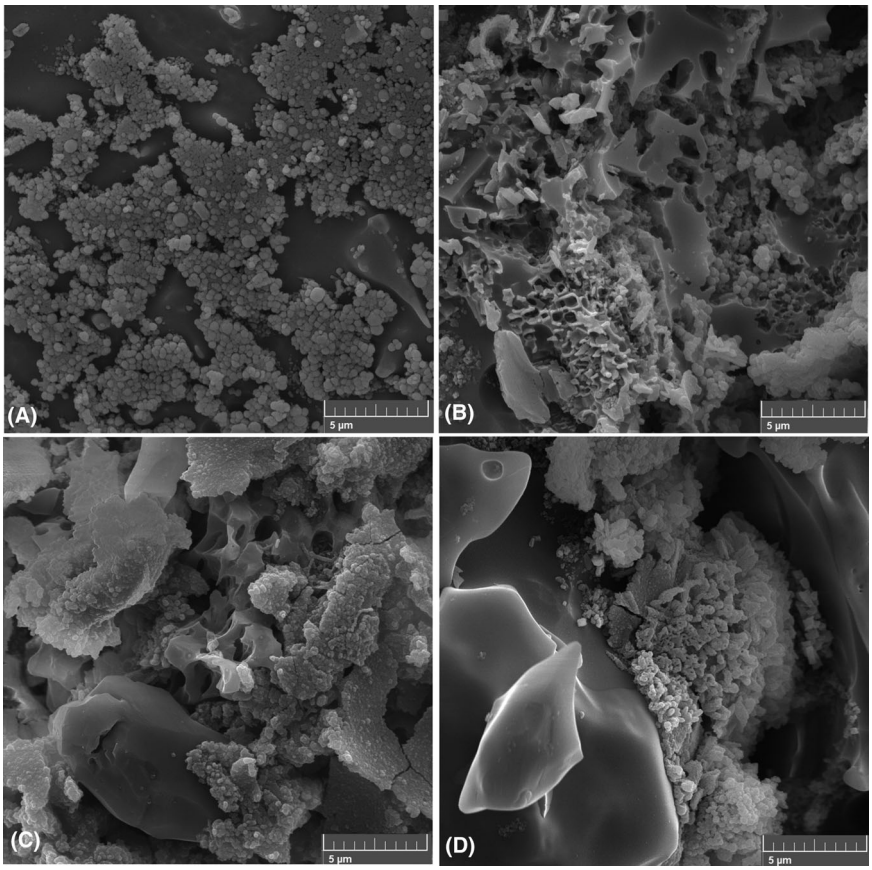

FIGURE 10 Field emission gun scanning electron microscopy (FEGSEM) of the porcelains obtained in this study: (A) experiment 1; (B) experiment 2; (C) experiment 3; and (D) experiment 4

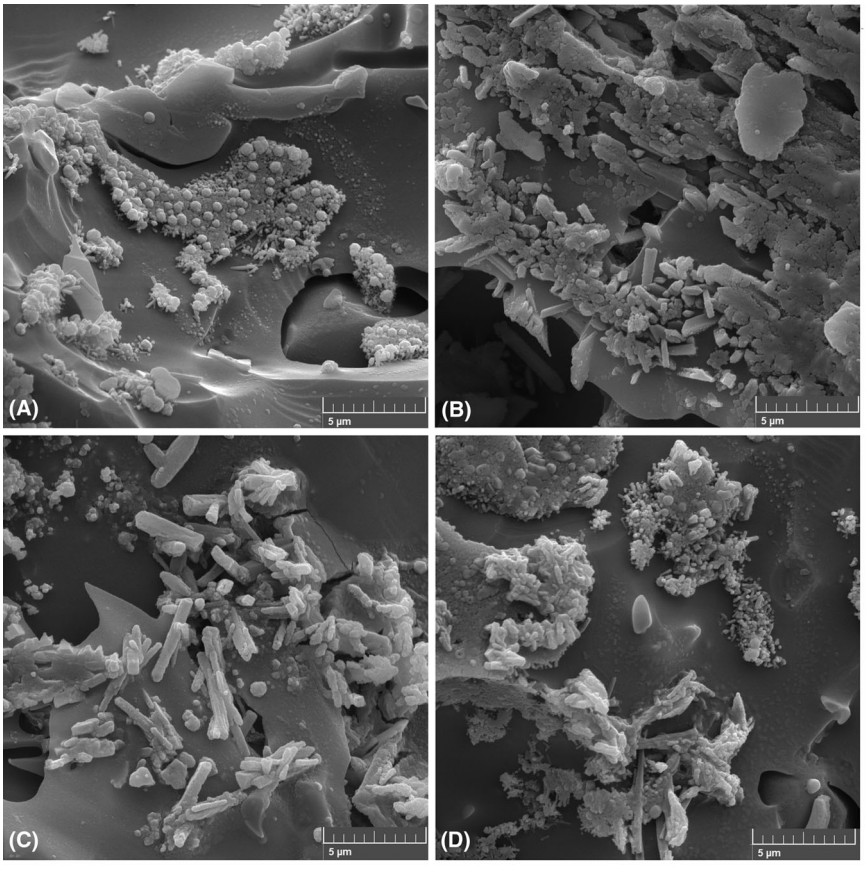

FIGURE 11 Field emission gun scanning electron microscopy (FEGSEM) of the porcelains obtained in this study: (A) experiment 5; (B) experiment 6; (C) experiment 7; and (D) experiment 8

TABLE 8 Chemical analysis of sintered samples (%wt.)

	Na_2O (%)	K_2O (%)	MgO (%)	CaO (%)	Al_2O_3 (%)	Fe_2O_3 (%)	SiO_2 (%)
Experiment 1	5.966	.651	1.463	.448	27.600	.697	63.175
Experiment 2	4.484	.650	3.303	.606	26.370	1.149	63.438
Experiment 3	5.001	.732	1.550	.594	26.547	1.048	64.528
Experiment 4	4.287	.643	4.076	1.251	24.601	1.288	63.854
Experiment 5	5.366	.626	1.416	.452	27.305	.805	64.030
Experiment 6	4.814	.608	2.523	.464	26.427	.954	64.210
Experiment 7	5.204	.632	1.364	.419	26.784	.709	64.888
Experiment 8	5.114	.611	3.053	.444	26.639	.844	63.295

lower intensity of the observed peaks, mainly in the albite phase consumed to promote the formation of the liquid phase during firing. In addition, there is a higher amount of amorphous band in the diffractograms (Figure 9), which is due to the greater formation of the glassy phase, as explained in the previous sections.

3.5 | Field emission gun scanning electron microscopy (FEGSEM) and chemical microanalysis by energy-dispersive X-ray spectroscopy (EDS)

Figures 10 and 11 present the images of the porcelains in experiments 1, 2, 3, 4 and 5, 6, 7, 8, respectively, with a magnification of 10 000 times.

It is possible to verify in the presence of a matrix composed of the vitreous phase in addition to a minority phase composed of small grouped lamellae, which can be associated with the primary mullite. Despite the microscopic analysis demonstrating the presence of mullite, its proportion was probably below the detection range of the equipment used in XRD (3%), for this reason this phase was not detected in the diffractograms. It can also be seen some quartz crystals. In agreement with the presented in XRD, the presence of secondary mullite in proportions above the detection limit of the equipment was also not evidenced in any sample. However, a magnification of 35 000 times (Figure 12) allowed the visualization of small needle-shaped prismatic crystals nucleating from the vitreous phase, which can be related to a small formation of this phase.[24,25]

Table 8, Figures 13, and 14 show the EDS microanalysis results of the compositions in all experiments carried out. The experiments in Figure 13, sintered at 1170°C (experiments 1–4), showed a surface with higher irregularity and porosity than the images in Figure 14 (experiments 4–7). They were sintered at 1220°C and therefore showed more formation of the glassy phase.

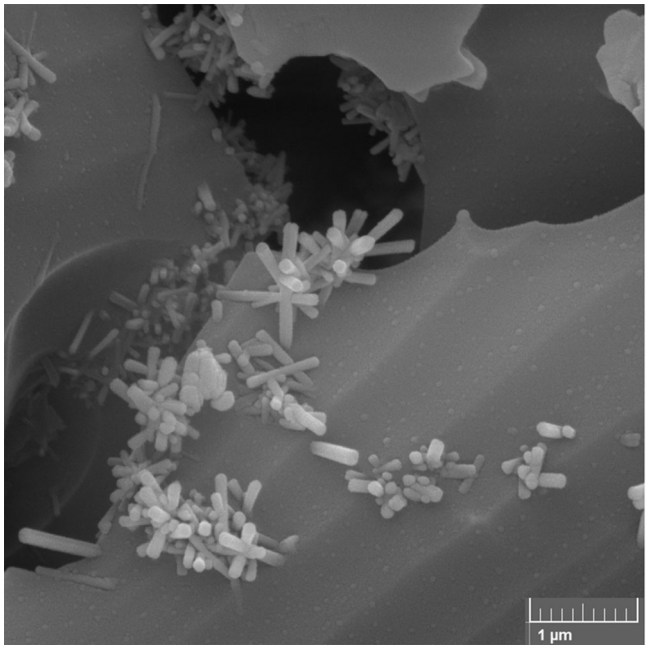

FIGURE 12 Field emission gun scanning electron microscopy (FEGSEM) of the sample obtained in experiment 2 in which the nucleation of small secondary mullite crystals from the glassy phase can be seen

Analyzing and Figure 13, in general, the elements were well distributed in the samples, except for some points with a higher concentration of magnesium and calcium, which are more pronounced in experiments 2 and 4 (where there was a higher addition of talc). However, no crystalline phases associated with these elements were found within the XRD detection limits, according to Figures 8 and 9. As expected, experiments 2 and 4 showed a higher proportion of MgO than experiments 1 and 3 (Table 8).

The experiments shown in Figure 14 showed calcium well distributed in the samples. This could have happened because the higher sintering temperature could have caused the calcium oxide to react within the composition. However, as its proportion is small, it cannot be said

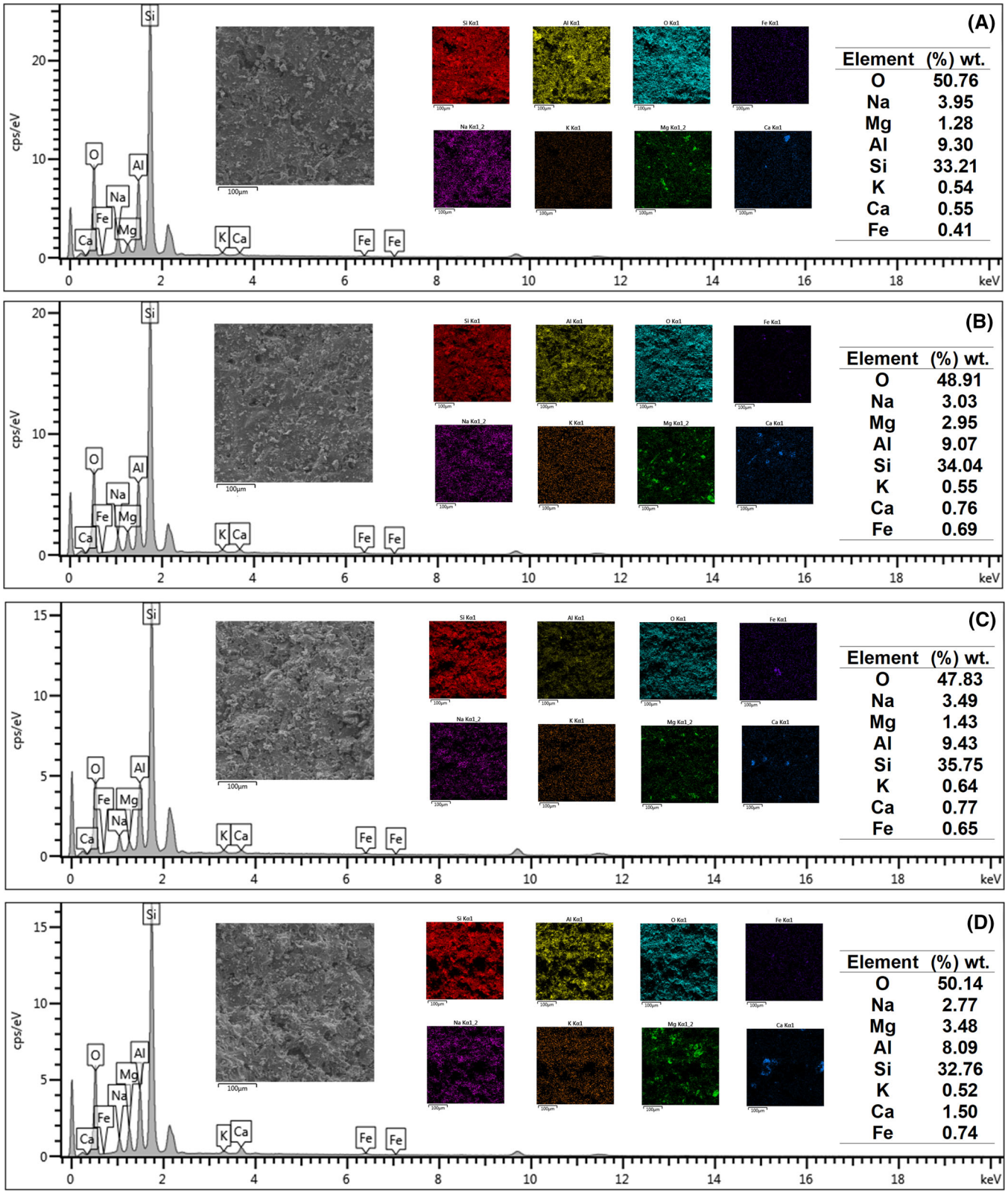

FIGURE 13 Chemical microanalysis of the porcelains obtained in this study: (A) experiment 1; (B) experiment 2; (C) experiment 3; and (D) experiment 4

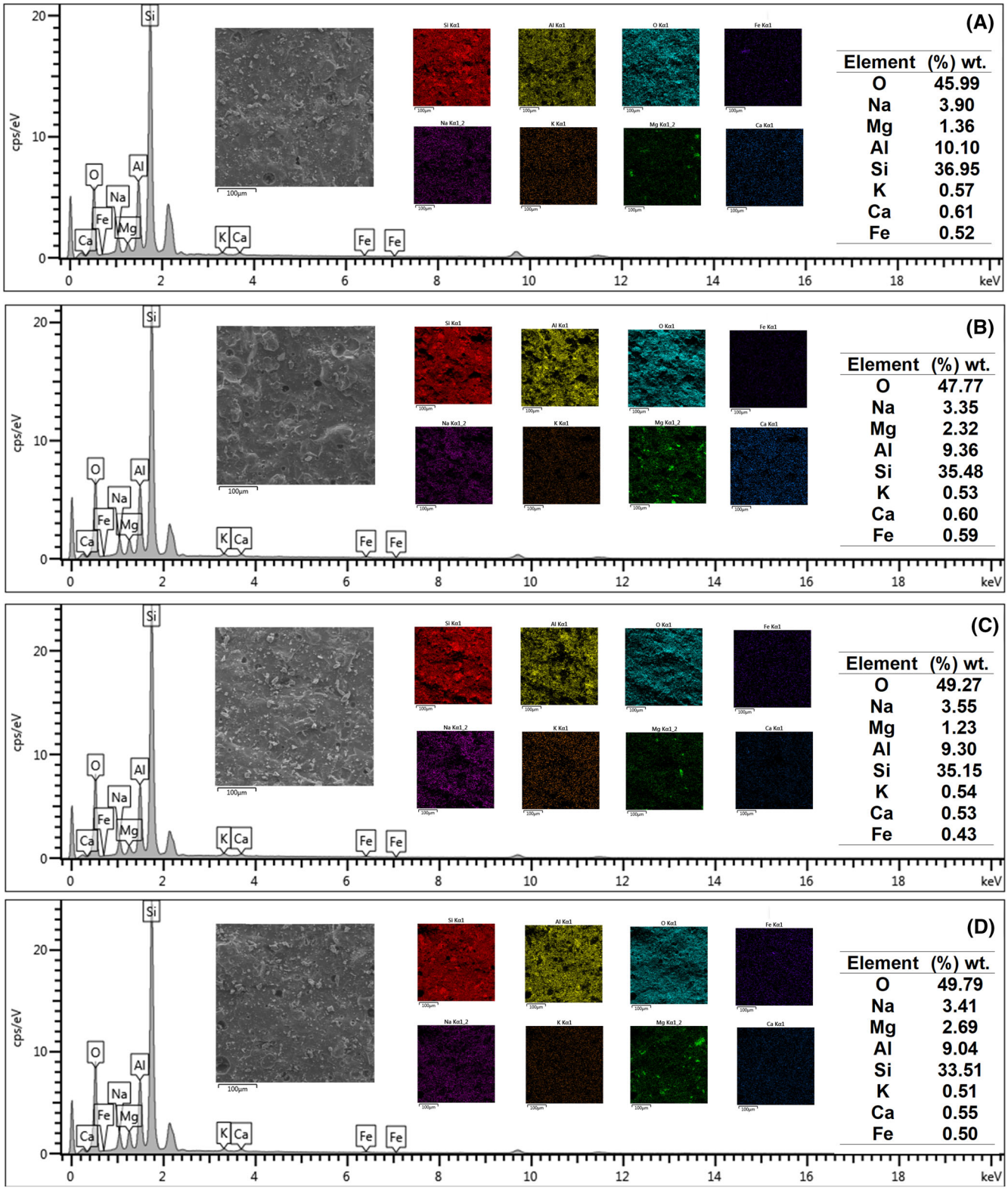

FIGURE 14 Chemical microanalysis of the porcelains obtained in this study: (A) experiment 5; (B) experiment 6; (C) experiment 7; and (D) experiment 8

with certainty whether it was incorporated into the glass phase lattice or remained in a minor crystalline phase that could not be detected. The other characteristics followed the same behavior discussed in Figure 13.

4 | CONCLUSION

From the data obtained by the factorial model, it was verified that temperature was the parameter that most influenced the gresification of the different samples produced, and it was only possible a greater densification at temperatures of 1220°C. The more refined initial talc granulometry was detrimental to total porosity when combined with higher talc proportions at the lower temperature. The presence of iron oxide in talc may provide higher color difference in samples with 20% of this raw material.

In general, the elevation of the sintering temperature and the talc proportion reduction beneficially increased the samples' mechanical strength. Hence, the more refined initial talc granulometry leads to a significant improvement in mechanical strength at 1170°C but at 1220°C promotes a principle of overfire damaging this property. We conclude that Itajara talc allowed the obtaining of parts with low porosity proportions, confirming its possibility as a flux agent of outstanding importance for the ceramic industry.

AUTHOR CONTRIBUTIONS

Conceptualization; experimentation; analysis; writing: Robson Couto da Silva. *Conceptualization; writing*: Felipe de Almeida La Porta. *Experimentation*: Graciela Aparecida Santos Silva. *Experimentation*: Renato Mandalozzo Tebcherani. *Conceptualization; analysis; methodology*: Evaldo Toniolo Kubaski. *Resources; experimentation; analysis*: Estevam Augusto Bonfante. *Conceptualization; experimentation; resources; approval; funding acquisition*: Sergio Mazurek Tebcherani.

ACKNOWLEDGMENTS

The authors gratefully acknowledge the financial support of CNPq (Brazil's National Council for Scientific and Technological Development), through grant numbers: 304675/2016-4 and 313484/2019-8.

CONFLICTS OF INTEREST

The authors declare that they have no known conflicts of interest or personal relationships that could have appeared to influence the work reported in this paper. All authors also confirm that they accept the insertion of the author Estevam Augusto Bonfante, who contributed to the accomplishment of the analyzes.

ORCID

Robson Couto da Silva https://orcid.org/0000-0002-2857-0182

Evaldo Toniolo Kubaski https://orcid.org/0000-0002-5238-8305

Estevam Augusto Bonfante https://orcid.org/0000-0001-6867-8350

Sergio Mazurek Tebcherani https://orcid.org/0000-0001-9601-448X

REFERENCES

1. Dondi M, Raimondo M, Zanelli C. Clays and bodies for ceramic tiles: reappraisal and technological classification. Appl Clay Sci. 2014;96:91–109. https://doi.org/10.1016/j.clay.2014.01.013
2. Calderón YER, Rangel CAN, Pla JL, Albert EB, Rios JSV, Castelló JBC. Development of ceramic porcelain stoneware pastes by the revalorization of Colombian clays subjected to bleaching process. Appl Clay Sci. 2019;178:105128. https://doi.org/10.1016/j.clay.2019.105128
3. Sanz A, Bastida J, Caballero A, Kojdecki MA. Microstructural analysis (Voigt function method) of mullite in whiteware triaxial porcelains. Appl Clay Sci. 2020;198:105805. https://doi.org/10.1016/j.clay.2020.105805
4. Njindam OR, Njoya D, Mache JR, Mouafon M, Messan A, Njopwouo D. Effect of glass powder on the technological properties and microstructure of clay mixture for porcelain stoneware tiles manufacture. Constr Build Mater. 2018;170:512–9. https://doi.org/10.1016/j.conbuildmat.2018.03.069
5. Gulgonul I, Çelik MS. Understanding the flotation separation of Na and K feldspars in the presence of KCl through ion exchange and ion adsorption. Miner Eng. 2018;129:41–6.https://doi.org/10.1016/j.mineng.2018.08.038
6. Dondi M. Feldspathic fluxes for ceramics: Sources, production trends and technological value. Resources, conservation and recycling. 2018;133:191–205. https://doi.org/10.1016/j.resconrec.2018.02.027
7. Larsen E, Johannessen NE, Kowalczuk PB, Kleiv RA. Selective flotation of K-feldspar from Na-feldspar in alkaline environment. Miner Eng. 2019;142:105928. https://doi.org/10.1016/j.mineng.2019.105928
8. Rodríguez-Ruiz MD, Abad I, Bentabol M, Cruz MDR. Evidences of talc-white mica assemblage in low-grade metamorphic rocks from the internal zone of the Rif Cordillera (N Morocco). Appl Clay Sci. 2020;195:105723. https://doi.org/10.1016/j.clay.2020.105723
9. Dzulkafli HH, Ahmad F, Ullah S, Hussain P, Mamat O, Megat-Yusoff PSM. Effects of talc on fire retarding, thermal degradation and water resistance of intumescent coating. Appl Clay Sci. 2017;146:350–61. https://doi.org/10.1016/j.clay.2017.06.013
10. Terzić A, Pezo L, Andrić L, Arsenović M. Effects of mechanical activation on the parameters of talc quality for ceramics production – chemometric approach. Composites Part B: Eng. 2015;79:660–6. https://doi.org/10.1016/j.compositesb.2015.05.022
11. Ober JA. Mineral commodity summaries 2018. In: Mineral commodity summaries. Reston, VA: U.S. Geological Survey; 2018. p. 204.

12. Torres HSS, Varajão AFDC, Sabioni ACS. Technological properties of ceramic produced from steatite (soapstone) residues–kaolinite clay ceramic composites. Appl Clay Sci. 2015;112–113:53–61. https://doi.org/10.1016/j.clay.2015.04.016
13. Sánchez E, Sanz V, Cañas E, Sales J, Kayacı K, Taşkıran MU, et al. Revisiting pyroplastic deformation. Application for porcelain stoneware tile bodies. J Eur Ceram Soc. 2019;39(2):601–9. https://doi.org/10.1016/j.jeurceramsoc.2018.09.032
14. Mukhopadhyay TK, Das M, Ghosh S, Chakrabarti S, Ghatak S. Microstructure and thermo mechanical properties of a talc doped stoneware composition containing illitic clay. Ceram Int. 2003;29(5):587–97. https://doi.org/10.1016/S0272-8842(02)00206-7
15. Serra MF, Picicco M, Moyas E, Suárez G, Aglietti EF, Rendtorff NM. Talc, spodumene and calcium carbonate effect as secondary fluxes in triaxial ceramic properties. Procedia Mater Sci. 2012;1:397–402. https://doi.org/10.1016/j.mspro.2012.06.053
16. da Silva AL, Feltrin J, Dal Bó M, Bernardin AM, Hotza D. Effect of reduction of thickness on microstructure and properties of porcelain stoneware tiles. Ceram Int. 2014;40(9 Part B):14693–9. https://doi.org/10.1016/j.ceramint.2014.05.150
17. Valášková M, Hundáková M, Smetana B, Drozdová Ľ, Klemm V, Rafaja D. Cordierite/CeO_2 ceramic nanocomposites from vermiculite with fixed CeO_2 nanoparticles, talc and kaolin. Appl Clay Sci. 2019;179:105150. https://doi.org/10.1016/j.clay.2019.105150
18. Magagnin D, dos Santos CMF, Wanderlind A, Jiusti J, De Noni A. Effect of kaolinite, illite and talc on the processing properties and mullite content of porcelain stoneware tiles. Mater Sci Eng: A. 2014;618:533–9. https://doi.org/10.1016/j.msea.2014.09.049
19. Güngör F, Ay N. The effect of particle size of body components on the processing parameters of semi transparent porcelain. Ceram Int. 2018;44(9):10611–20. https://doi.org/10.1016/j.ceramint.2018.03.086
20. Gültekin EE, Topateş G, Kurama S. The effects of sintering temperature on phase and pore evolution in porcelain tiles. Ceram Int. 2017;43(14):11511–5. https://doi.org/10.1016/j.ceramint.2017.06.024
21. Box GEP, Hunter WG, Hunter JS. Statistics for experimenters: an introduction to design, data analysis, and model building. 1 ed. New York: John Willey & Sons; 1978. p. 652.
22. Bernasconi A, Diella V, Pagani A, Pavese A, Francescon F, Young K, et al. The role of firing temperature, firing time and quartz grain size on phase-formation, thermal dilatation and water absorption in sanitary-ware vitreous bodies. J Eur Ceram Soc. 2011;31(8):1353–60. https://doi.org/10.1016/j.jeurceramsoc.2011.02.006
23. Martín-Márquez J, Rincón JM, Romero M. Effect of microstructure on mechanical properties of porcelain stoneware. J Eur Ceram Soc. 2010;30(15):3063–9. https://doi.org/10.1016/j.jeurceramsoc.2010.07.015
24. Güngör F. Investigation of pyroplastic deformation of whitewares: effect of crystal phases in the ''CaO'' based glassy matrix. Ceram Int. 2018;44(11):13360–6. https://doi.org/10.1016/j.ceramint.2018.04.169
25. Ochen W, D'ujanga FM, Oruru B, Olupot PW. Physical and mechanical properties of porcelain tiles made from raw materials in Uganda. Results Mater. 2021;11:100195. https://doi.org/10.1016/j.rinma.2021.100195

How to cite this article: da Silva RC, La Porta FA, Silva GAS, et al. Application of factorial model for an optimization of partial replacement of feldspar by talc on the sintering process. Int J Appl Ceram Technol. 2023;20:1576–1590. https://doi.org/10.1111/ijac.14332